INTERNATIONAL JOURNAL FOR NUMERICAL METHODS IN ENGINEERING, VOL. 39, 635–661 (1996)

NUMERICAL SMEARED FRACTURE ANALYSIS: NONLOCAL MICROCRACK INTERACTION APPROACH

JOŠKO OŽBOLT

Institut für Werkstoffe im Bauwesen, Stuttgart University, Stuttgart, Germany

ZDENĚK P. BAŽANT

Walter P. Murphy Professor of Civil Engineering and Materials Science, Northwestern University, Evanston, IL 60208, U.S.A.

SUMMARY

A recently proposed new nonlocal concept based on microcrack interactions is discussed, its implementation in a smeared cracking finite element code for concrete is presented, numerical studies are reported, and comparisons with experimental results are made. The nonlocality is not merely a mathematical device to prevent excessive spurious localization into a zone of zero volume but is a necessary physical consequence of microcrack interactions. Since the constitutive law itself is strictly local, the new nonlocal concept can be combined with any type of constitutive law for strain-softening nonlocal damage, which is here chosen to be the microplane model. A simple method is formulated to approximately identify the material parameters in the model from the basic characteristics of concrete such as the tensile strength, fracture energy and maximum aggregate size. The results of finite element analysis are shown to be mesh insensitive, and good convergence is obtained. Cracking damage is found to localize into a volume whose size and shape depend on the macroscopic concrete properties as well as the current stress–strain state. Although the damage is considered to be tensile on the microlevel, due solely to mode I microcracks, the new nonlocal model can describe well not only mode I fracture tests but also complex shear-dominated and mixed-mode types of failure such a diagonal shear, and can do so for the same values of material parameters (which was not the case for previous nonlocal models). Most importantly, the new nonlocal model can correctly capture the size effect of quasibrittle fracture, in approximate agreement with Bažant's size effect law.

KEY WORDS: fracture; damage; microcracking; finite element analysis; nonlocal models; concrete structures

1. INTRODUCTION

More than a decade ago, the nonlocal continuum concept was proposed as a general way to avoid spurious mesh sensitivity and excessive localization in macroscopic modelling of fracture process in quasi-brittle materials such as concrete, rocks, tough ceramics and fibre composites.[1,35] Although most of the finite element codes in engineering practice are still based on the classical local continuum approach to smeared cracking, there is now much evidence that the local finite element codes, even those based on the partially nonlocal crack band approach,[2,3] often cannot simulate brittle failures of concrete structures correctly.[4–6] To suppress spurious mesh sensitivity and excessive localization and, most importantly, to capture the size effect, the finite element code must contain a mathematical device called the localization limiter, which prevents from localizing damage into a zone of zero volume. Alternatively, correct prediction often can also be obtained by a discrete cohesive crack approach characterized by a softening crack-bridging law.

CCC 0029–5981/96/040635–27
© 1996 by John Wiley & Sons, Ltd.

Received 14 September 1994
Revised 6 February 1995

This alternative approach, however, seems less versatile in general situations than a nonlocal code with smeared cracking.

A continuum model for a brittle heterogeneous material such as concrete must correctly represent the consequences of distributed defects due to heterogeneity of the microstructure. The defects such as microcracks or damage sites interact. Two types of interactions exist and must be somehow represented in the continuum model: (1) Interaction at distance among various sites, and (2) interaction among various orientations. The latter interaction controls non-linear triaxial constitutive behaviour and is most directly handled by the microplane model.[7,37] The interaction at distance controls localization of damage. It is ignored by the classical, local continuum models, but is taken into account in the nonlocal models. In these models, the stress at a point depends not only on the strain at the same point but also on the strain field within a certain neighbourhood of the point—an idea that was introduced for elastic deformations already by Eringen[8,9] and Kröner.[10] For strain softening behaviour, this concept was introduced by Bažant.[1,11]

An effective form of the nonlocal concept, in which all the variables associated with strain softening are nonlocal and all the others are local, was introduced by Pijaudier-Cabot and Bažant.[12,36] The governing parameter in this concept is the characteristic length l over which the strains are averaged. This length has a major influence on the results of analysis, especially on the size effect.[6,13]

Initially it was assumed that l is a material parameter of concrete that can be correlated to the maximum aggregate size d_a, perhaps roughly as $l = 3d_a$. However, now it is clear that, in general applications, l cannot be correlated to the parameters of the concrete mix alone, but is influenced by other parameters as well. It has been demonstrated[14] that the optimum values of ratio l/d_a, identified in numerical simulations using the previous nonlocal form of the microplane material model, change significantly from one type of problem to another, for example, from tensile fracture specimen to anchor pullout or diagonal shear failure of a beam. Such variation could not be explained by differences in the composition of concrete. Aside from that, recent theoretical work[15,16] also confirmed that l is not a material constant but a material function depending on the strain and stress field in the neighbourhood of a point in the fracture process zone.

For characteristic length equal to the element size, the nonlocal approach degenerates into the crack band approach.[2] In that approach one must adjust the local strain-softening behaviour such that the area under the tensile stress–strain curve multiplied by the average element size (crack band width) be equal to the fracture energy of concrete, G_f. Imposition of this condition does ensure objectivity (mesh-size insensitivity) when the mesh line coincides with the fracture path, but in general the analysis is still quite mesh dependent (initially, it was thought that arbitrary crack paths can be handled in the form of zig-zag crack bands, but this is now known to cause significant errors and bring about problems such as stress locking).

The fracture process zone in concrete has a non-zero and variable size and variable shape, depending on the surrounding stress–strain field. Simple adaptation of the area under the tensile stress–strain curve for the elements in the crack band cannot adequately capture the variations of the fracture process zone, especially for various directions of the fracture path relative to the mesh lines. The crack band approach is a simple but scalar concept, and this is a severe limitation in general situations.

In view of the foregoing picture, a nonlocal concept for smeared cracking analysis is inevitable. It is also dictated by the physical process of fracture. Recently it has been demonstrated that the nonlocality is a necessary consequence of microcrack interactions.[17] A new special form of the nonlocal concept that is deduced from the interaction of growing microcracks has been developed.

In the present study, this new nonlocal concept will first be reviewed and discussed. Then its implementation into a large finite element code with the microplane constitutive model will be presented. Identification of the basic material parameters involved will be studied, numerical examples will be presented, and comparisons with experimental data will be made.

2. NONLOCALITY DUE TO MICROCRACK INTERACTIONS

Softening in a quasi-brittle material, such as concrete, is a consequence of the fact that many microcracks develop in the fracture process zone before a major continuous macrocrack is produced. Because of the randomness of microcracks as well as material heterogeneity, the material must be regarded as a random disordered material. The macro-continuum model for such a material cannot be written in the classical, local form in which the stress tensor $\boldsymbol{\sigma}$ at any given point is a function of the strain tensor $\boldsymbol{\varepsilon}$ at the same point. Rather, $\boldsymbol{\sigma}$ must be considered to be a function of the strain field in the neighbourhood of the given point. In the original nonlocal approach, the inelastic part of $\boldsymbol{\sigma}$ is assumed to be a function of the spatial weighted average of $\boldsymbol{\varepsilon}$ within a certain characteristic neighbourhood of the point, called the nonlocal strain $\bar{\boldsymbol{\varepsilon}}$. A more sophisticated, physically based nonlocal concept, reflecting in a certain special way the interactions among the microcracks randomly distributed in the material will be used in this paper, based on a recent formulation derived by Bažant.[18]

Because on the microlevel the material between the microcracks is assumed to be elastic, Bažant[17] proposed to calculate the response of the microcracked continuum on the basis of the superposition principle, which has been used for discrete crack systems by Collins[19] (with displacements as unknowns), Kachanov[20,21] (with crack pressures as unknowns) and others. According to this principle, each loading step is decomposed in two substeps:

1. In the first substep, the strain increment $\Delta\boldsymbol{\varepsilon}$ (Figure 1) is applied imagining all the microcracks to be temporarily closed (as if glued or frozen) and the stress increment $\Delta\boldsymbol{\sigma}$ is easily calculated as the elastic stress increment, which implies the microcracks to be able to transfer the stresses.

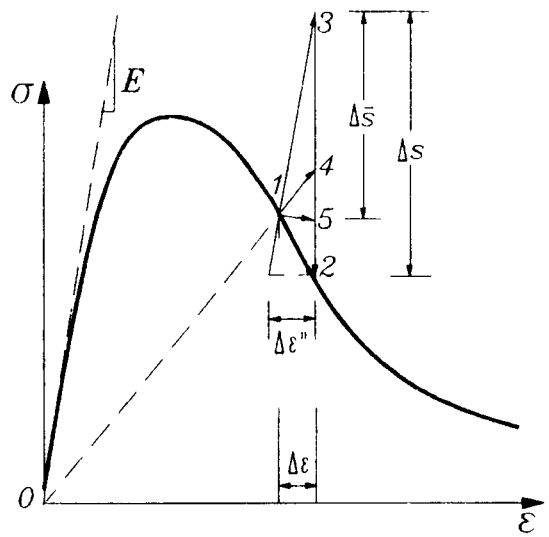

Figure 1. Local and nonlocal inelastic stress increments for known strain increment

2. In the second substep, the stresses transmitted between the microcrack surfaces are relaxed (as if the cracks were unglued or unfrozen). This is equivalent to applying pressure on the crack surfaces.

If, during the load step, no crack would grow due to the unglueing (unfreezing) in substep 2, one would get the stress drop $\overline{34}$ shown in Figure 1. But because in general the cracks grow, a larger stress drop $\Delta S = \overline{32}$ takes place. This stress drop is defined by the local stress-strain law, which is the law describing a material element that can be deformed homogeneously in the macroscopic sense. However, the crack opening and growth (or closing) at one macro-continuum point generally causes crack opening and growth (or closing) at another macro-continuum point, because the microcracks interact. Due to this interaction, the actual stress drop is different, as shown by $\Delta\bar{S} = \overline{35}$ in Figure 1, and is called the nonlocal stress increment. If $\Delta\mathbf{S}_\mu$ represents the local inelastic stress increment tensor at the location of microcrack number μ, then the normal traction (pressure) applied at the crack surfaces of microcrack number μ is:

$$\Delta p_\mu = \mathbf{n}_\mu \Delta\mathbf{S}_\mu \mathbf{n}_\mu \tag{1}$$

where $\mathbf{n}_\mu$ = unit normal to the surfaces of microcrack μ. Since Δp_μ represents only a local pressure (traction) drop at location μ, the stress drop due to the unglueing of microcracks at other adjacent locations ν must be added. Together with two important simplifications,[17] namely: (1) uniformity of stress Δp_μ along the crack surface (justified by Kachanov[20,21]) and (2) consideration of mode I crack openings only, the superposition principle then provides for the total nonlocal inelastic stress increment $\Delta\bar{p}_\mu$ the following relation (introduced by Kachanov):[21]

$$\Delta\bar{p}_\mu = \langle \Delta p_\mu \rangle + \sum_{\nu \neq \mu} \Lambda_{\mu\nu} \Delta\bar{p}_\nu \tag{2}$$

Here $\langle \cdots \rangle$ is the averaging operator over the crack length ($\mu = 1, \ldots, N$, $\nu = 1, \ldots, N$ with N = total number of microcracks) and $\Lambda_{\mu\nu}$ are the crack influence coefficients representing the average pressure at the glued (frozen) target microcrack μ caused by a unit uniform pressure applied on the surfaces of an unglued (unfrozen) source microcrack ν, with all other microcracks being glued (frozen). In consequence of Kachanov's[22] approximation for discrete microcrack systems, instead of the local stress increment Δp_μ, one may use in (2) the local stress increment $\langle \Delta p_\mu \rangle$ averaged over the surface of the target microcrack. Introducing (1) into (2), it follows that[17]

$$\Delta(\mathbf{n}_\mu \bar{\mathbf{S}}_\mu \mathbf{n}_\mu) = \langle \Delta(\mathbf{n}_\mu \mathbf{S}_\mu \mathbf{n}_\mu) \rangle + \sum_{\nu=1}^{N} \Lambda_{\mu\nu} \Delta(\mathbf{n}_\nu \bar{\mathbf{S}}_\nu \mathbf{n}_\nu) \tag{3}$$

Note that $\Lambda_{\mu\mu} = 0$ since interaction of a crack with itself has no physical meaning.

Equation (3) must be adapted for smeared cracking on the macro-continuum level. To do this, Bažant[17] introduced two simplifying hypotheses: (1) The influence of the microcracks at point $\boldsymbol{\xi}$ of the macro-continuum upon the microcracks at point $\mathbf{x}$ (Figure 2) is determined only by the dominant microcrack orientation at each point, which is assumed to be normal to the current direction of total maximum principal strain $\varepsilon^{(1)}$ (it might be more logical to assume it to be normal to the maximum principal direction of $\bar{\mathbf{S}}$, but this would be more complicated in programming and the difference would probably be unimportant); and (2), rather than working with tractions perpendicular to the individual random microcracks, one may work with tractions whose direction is defined on the macro-level. Based on these assumptions, (3) may be adapted to

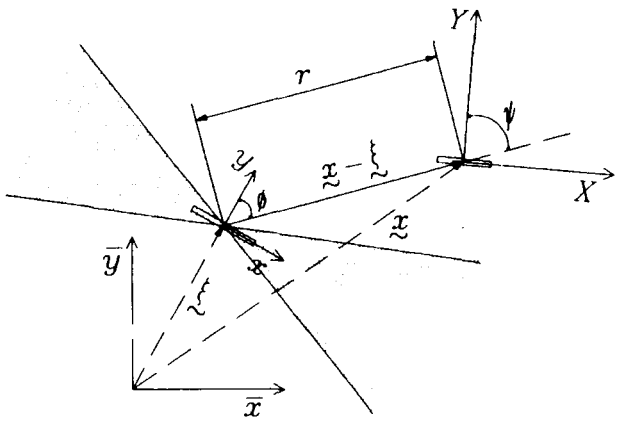

Figure 2. Interaction between two discrete microcracks of different orientations (the shaded zones indicate areas with positive crack interaction function)

a continuum form by replacing the discrete sum with an integral. This yields[17]

$$\Delta\bar{S}^{(1)}(\mathbf{x}) = \langle \Delta S^{(1)}(\mathbf{x}) \rangle + \int_V \Lambda(\mathbf{x}, \xi)\, \Delta\bar{S}^{(1)}(\xi)\, \mathrm{d}V(\xi) \tag{4}$$

where $\Delta\bar{S}^{(1)}(\mathbf{x})$ and $\Delta S^{(1)}(\mathbf{x})$ are the nonlocal and local inelastic stress increments in the direction normal to the dominant microcrack orientation, and $\Lambda(\mathbf{x}, \xi)$ is the crack influence function characterizing microcrack interactions in the given body, determined from the stress field of one crack in the body of given geometry. For the sake of simplicity, however, we will later use function $\Lambda(\mathbf{x}, \xi)$ corresponding to a crack in an infinite body and modify it in an approximate manner to take into account the effect of boundaries. Because the structure is much larger than the microcracks, such a modification will be necessary only for points near the boundaries.

Note that the micro–macro transition from (3) to (4) has not been effected by a homogenization technique. These classical techniques for elastic constants cannot be used because they apply only to statistically homogeneous states, i.e., uniform macrostrain field.

In the finite element formulation, the integral in (4) is approximated by a sum running over the coordinates of integration points of all finite elements (instead of individual microcracks);

$$\Delta\bar{S}_\mu^{(1)} = \langle \Delta S_\mu^{(1)} \rangle + \sum_{\nu=1}^{N} \Lambda_{\mu\nu} \Delta\bar{S}_\nu^{(1)} \Delta V_\nu \tag{5}$$

where ΔV_ν = part of finite element volume corresponding to integration point ν. The subscripts μ and ν now label the coordinates of the integration points rather than the microcracks. Over an infinite body, the integral of $\Lambda(\mathbf{x}, \xi)$ has been shown to be zero (provided a certain integration path is excluded, as explained in Reference 17).

As can be seen from (4) and (5), the nonlocal inelastic stress increment $\Delta\bar{S}_\mu^{(1)}$ consists of the inelastic stress increment arising from microcrack interactions (which are long-range), and the average local inelastic stress increment $\langle \Delta S_\mu^{(1)} \rangle$, which is obtained by short-range averaging of the local inelastic stress increments over a domain of about the same size as the microcrack. The averaging operator $\langle \cdots \rangle$ introduced in (3) is reflected on the macro-level by averaging of the microcrack surface tractions over the microcrack. However, in smeared crack analysis, there is no crack, and so one must average over a volume instead of the microcrack surface. We assume this averaging volume to be of about the same size as the dominant microcracks, which is about the

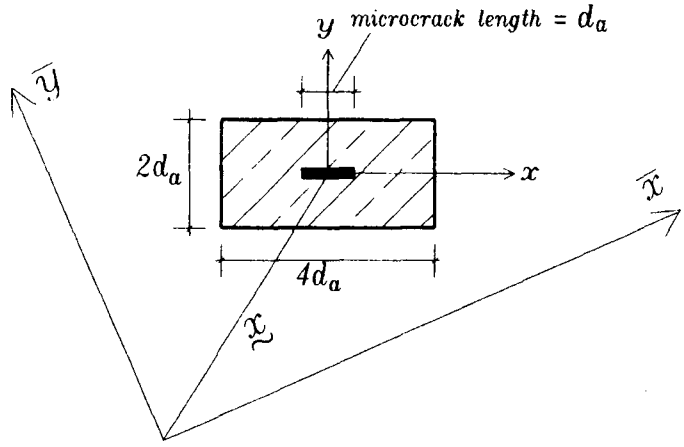

Figure 3. Local normalizing volume—its orientation and size

same as the aggregrate size. The averaging of the local inelastic stress increments introduced in (5), which reflects averaging over microcrack area, is performed as:

$$\langle \Delta S_\mu^{(1)} \rangle = \frac{1}{V_\mu} \sum_{v=1}^{n} \Delta S_v^{(1)} \alpha_{\mu v} \Delta V_v \tag{6}$$

where $V_\mu = \sum_{v=1}^{n} \alpha_{\mu v} \Delta V_v$ = local normalizing volume, n = number of all the integration points inside this volume and $\alpha_{\mu v}$ = weight coefficients whose distribution has a bell shape in both x and y directions, described by a polynomial of the fourth degree. The bell shape, which is similar to that in the nonlocal damage approach, is convenient for numerical reasons, giving smoother results than a rectangular weight distribution.[13] The size of V_μ is taken about the same as the maximum of one aggregate piece volume. For two-dimensional analysis, the region of averaging is taken as a rectangle with its longer side in the microcrack direction and its shorter side in the perpendicular direction (see Figure 3).

The long-range interaction in equations (4) and (5) is controlled by the crack interaction function, $\Lambda(\mathbf{x}, \xi)$. It adjusts the locally averaged inelastic stress increments as a consequence of microcrack openings or closings in the neighbourhood of each integration point. For the purpose of numerical analysis, some properties of the crack interaction function must be preserved while others must be simplified.[17] Preserved must be the long-range asymptotic form of the crack influence function. Simplified must be the close-range properties of this function because on the macroscale it is impossible to deal with randomly located microcracks of a finite size and the singularities at the crack tips must be smoothed out.

Assuming the body to be much larger than the microcracks, one can calculate the crack interaction function as the stress field of a crack in an infinite body, loaded by a unit uniform pressure $\sigma = 1$ on the crack surfaces. However, on the macrolevel, one must take into account the statistical distribution of the dominant microcracks. For this purpose, one may consider, as a simplified picture, the body to be subdivided into a regular array of cells the size of which is equal to the typical spacing of the dominant microcracks, which is approximately the same as the typical spacing s of the largest aggregate pieces. For the sake of simplicity, one may take these cells (in two dimensions) to be squares of size s, and in each cell there is one and only one microcrack whose centre occurs within the cell randomly, with a probability given by a weight function $w(x, y)$ that smoothly decreases toward the boundaries of the cell (this decrease approximately substitutes for the consideration of joint probability of occurrence of microcracks in

adjacent cells). By this reasoning, the following expression for the crack influence function has been obtained (Reference 17, Addendum):

$$\Lambda(0, \xi) = \frac{1}{s^2} \int_{-s/2}^{s/2} \int_{-s/2}^{s/2} w(x, y)\sigma^{(1)}(\xi - x, \eta - y)\,dx\,dy \tag{7}$$

where the origin of co-ordinates is placed into the centre of the $s \times s$ cell, axis x is normal to the crack, and $\sigma^{(1)}$ is the principal stress at point $\xi = (\xi, \eta)$ caused by a unit uniform pressure applied on the faces of a crack of length $2a$ centred at $\mathbf{x} = (x, y)$ (in more detail, see Reference 22).

As it turns out, the evaluation of the foregoing integral yields complicated expressions which need to be suitably simplified. This has not been achieved yet. However, an approximation proposed in Bažant[17] is probably adequate for most practical purposes. This approximation is based on the fact that the foregoing statistical averaging integral must preserve the long-range interactions exactly because, for a source crack and a target crack located in two remote cells, the rays connecting the cracks are about equally long and have about the same directions for all the possible random realizations of these cracks. The two- and three-dimensional long-range asymptotic fields for cracks in two and three dimensions have been determined from Westergaard's and Fabrikant's solutions, respectively.[23,24] For the former, this field may be written as:

$$\Lambda(\mathbf{x}, \xi) = k(r)f(\phi) \tag{8}$$

Here r and ϕ are polar co-ordinates with origin in the centre of a crack, ϕ being measured from the crack direction (see Figure 2); $\mathbf{x}$ is location of the centre of an unfrozen source microcrack on whose faces the unit pressure ($\sigma = 1$) is applied; and ξ is the location of the frozen target microcrack at which the stress perpendicular to the microcrack is calculated. As a consequence of elastic properties, function $\Lambda(\mathbf{x}, \xi)$ is symmetric with respect to interchanging $\mathbf{x}$ and ξ. Function k is found to be $k(r) = a^2/r^2$. It exhibits singularity at the source crack centre. Since in continuum analysis the short-range values have no meaning, it has been proposed to use (9) as an approximation for the entire space, but with a modified function $k(r)$ which preserves the long-range asymptotic field. For reasons stated in Bažant,[17] one may use for two dimensions the approximation:

$$k(r) = \left(\frac{\kappa l r}{r^2 + l^2}\right)^2 \tag{9}$$

and for three dimensions the approximation:

$$k(r) = \left(\frac{\kappa l r}{r^2 + l^2}\right)^3 \tag{10}$$

where l is an empirical constant which may be identified with what has been called the *characteristic length* of the nonlocal continuum,[12,36] and κ is an empirical parameter.

Because of crack growth, one might think that κ should be considered to increase as the dominant microcrack grows, and therefore, in numerical analysis, it should be correlated to the total principal strain, i.e., $\kappa = f(\varepsilon^{(1)}, L)$ where $\varepsilon^{(1)}$ = total maximum principal strain and L = constant related to the maximum aggregate size. However, because we take the local constitutive law for S as given (determined empirically from material test data), and because this law already takes into account the effect of the growth of dominant microcracks (under the assumption that they are all equally large and the macro-strain field is uniform), κ must be used as a constant, determined empirically. There are reasons to assume that the average microcrack length κl is proportional to the spacing of the major inhomogeneities (aggregate pieces), which in

turn is proportional to the maximum aggregate size d_a or to prevalent spacing of the major aggregrate pieces. In numerical implementation of the present model discussed later, good results are obtained with the assumption $\kappa l = d_a$.

The microcrack directions at two different locations $\mathbf{x}$ and ξ are generally not the same. Therefore, when a unit stress σ is applied perpendicular to the microcrack direction at location $\mathbf{x}$, $\Lambda(\mathbf{x}, \xi)$ represents the stress component normal to the microcrack at location ξ, i.e., $\Lambda(\mathbf{x}, \xi)$ should not only be a function of distance r between two microcracks, but also a function of their orientations. In the sense of (5), Λ is a scalar, and so different microcrack orientations can be taken into account simply by projecting the stress tensor obtained from the asymptotic form of Westergaard's or Fabrikant's solution for $\boldsymbol{\sigma} = 1$ at location $\mathbf{x}$ on the plane of the dominant microcrack at location ξ.[17]

A practically important property of function $\Lambda(\mathbf{x}, \xi)$ is its positive value in sectors about the microcrack direction and negative values in wide sectors about the normal to the microcrack (Figure 2). The negative values represent the phenomenon of shielding. In other words, the formation and growth of the source crack opposes the formation and growth of a target crack in these sectors. Finite element applications show that the shielding property is important for the correct representation of macro-crack propagation and, especially, the consumption of energy when many randomly distributed microcracks localize into a single macrocrack. The shielding is significant in a volume of diameter $D \approx 8\kappa l$ and, therefore, it affects long-range interactions. This helps significantly to obtain correct predictions of cracking when the finite element discretization is relatively coarse. It provides an important correction to the previous local finite element model.

3. GENERAL PROCEDURE AND ASSUMPTIONS OF FINITE ELEMENT IMPLEMENTATION

In finite element codes, non-linearity is usually treated by equilibrium iterations during the loading steps. Typically, for a given strain increment and material constitutive law, the stress increments in the local constitutive law are calculated for each integration point as

$$\Delta\boldsymbol{\sigma} = \mathbf{E}:(\Delta\boldsymbol{\varepsilon} - \Delta\boldsymbol{\varepsilon}'') = \mathbf{E}:\Delta\varepsilon - \Delta\mathbf{S} \tag{11}$$

in which $\Delta\boldsymbol{\sigma}$, $\Delta\boldsymbol{\varepsilon}$ = stress and strain increment tensors, $\mathbf{E}$ = fourth-rank tensor of elastic moduli of uncracked material, $\Delta\boldsymbol{\varepsilon}''$ = inelastic strain increment tensor, and $\Delta\mathbf{S}$ = inelastic stress increment tensor. The nonlocal formulation is obtained from (11) if the local inelastic stress increment tensor is replaced by the nonlocal one:

$$\Delta\boldsymbol{\sigma} = \mathbf{E}:(\Delta\boldsymbol{\varepsilon} - \Delta\boldsymbol{\varepsilon}'') = \mathbf{E}:\Delta\boldsymbol{\varepsilon} - \Delta\bar{\mathbf{S}} \tag{12}$$

where $\Delta\bar{\mathbf{S}}$ represents the nonlocal inelastic stress increment tensor. In classical nonlocal analysis, $\Delta\bar{\mathbf{S}}$ has been calculated by a spatial averaging integral.[12,13]

In the present nonlocal approach, $\Delta\mathbf{S}$ for each iteration step, each finite element and each integration point can be calculated using the given local constitutive law. The numerical implementation assumes that: (1) the dominant microcrack is opening, and thus interacting with another dominant microcrack, if and only if the inelastic stress increment normal to the microcrack direction is positive ($\Delta S^{(1)} > 0$, i.e., the crack grows); and (2) the microcrack is normal to the total principal strain direction. Interaction between two microcracks at locations μ and ν is considered only if both microcracks fulfill assumption (1), i.e., $\Delta S_\mu^{(1)}$ and $\Delta S_\nu^{(1)}$ are both positive. The direction of the maximum local inelastic stress increment generally does not coincide with the normal to the microcrack $\mathbf{n}_\mu$. Therefore, assumption 2 requires that the total inelastic stress

increment tensor $\Delta \mathbf{S}_\mu$ be projected on the direction normal to the microcrack $\mathbf{n}_\mu$. The maximum principal local inelastic stress increment in direction $\mathbf{n}_\mu$ is obtained as:

$$\Delta S_\mu^{(1)} = \Delta(\mathbf{n}_\mu \mathbf{S}_\mu \mathbf{n}_\mu) \tag{13}$$

Introducing $\Delta S_\mu^{(1)}$ into (5) and solving the system of N linear equations (where N = total number of integration points), one obtains $\Delta \bar{S}_\mu^{(1)}$. Replacing the local inelastic stress increment $\Delta S_\mu^{(1)}$ with the nonlocal $\Delta \bar{S}_\mu^{(1)}$ in the stress tensor $\Delta \mathbf{S}_\mu$, one gets the nonlocal stress increment tensor $\Delta \bar{\mathbf{S}}_\mu$. The subsequent procedure is the same as in any nonlinear finite element code, i.e. the iterations for the current load step are terminated when equilibrium between the nodal loads and nodal resisting forces is reached, with a prescribed tolerance of error. The flow chart of the procedure just explained is shown in Figure 4.

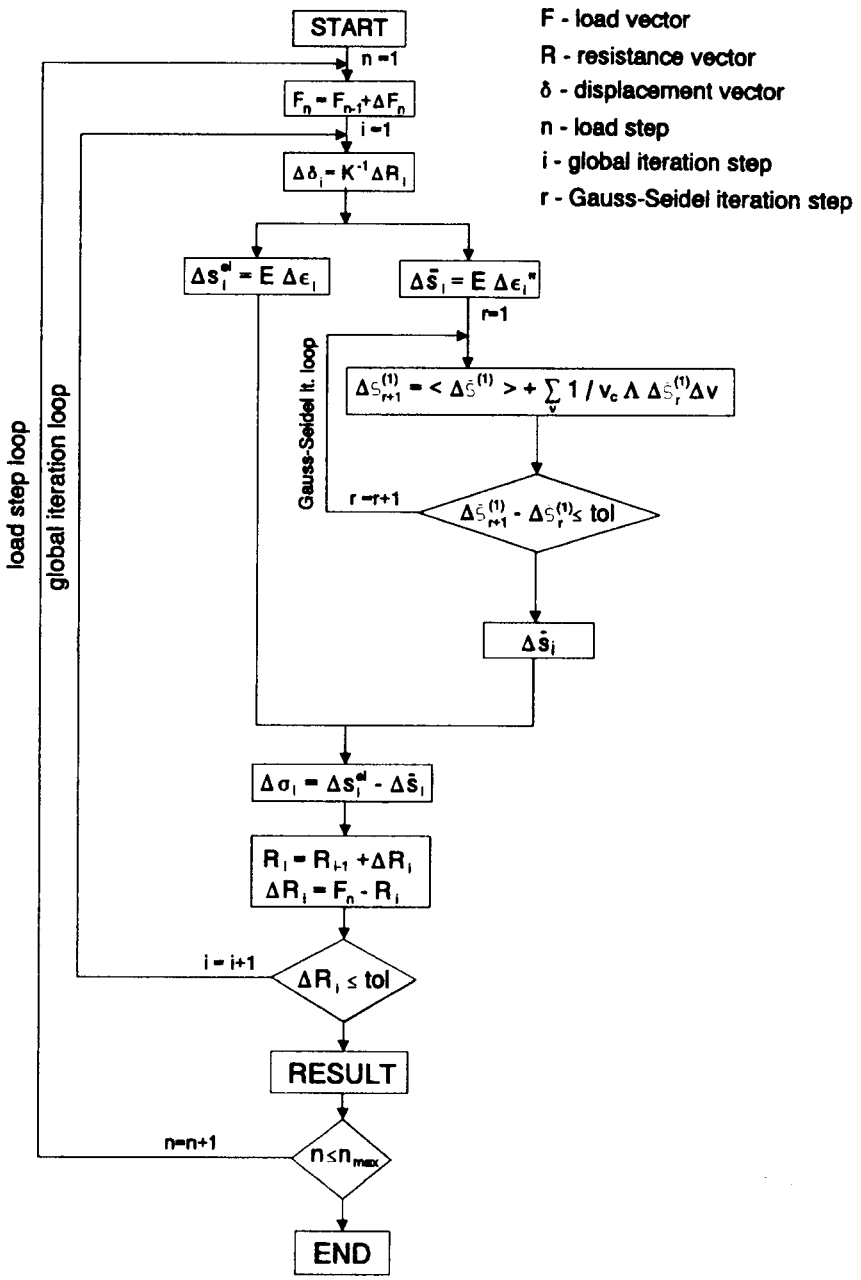

Figure 4. Flowchart of the numerical procedure employed in the finite element code

The crack influence function $\Lambda(\mathbf{x}, \xi)$ is implemented in a finite element code in the form of (8) with (9) or (10). To take into account the effect of different microcrack orientations, the stress tensor at point $\mathbf{x}$, calculated from the stress field produced by a unit normal stress applied on the surfaces of microcrack ξ (definition of the crack interaction function), is simply projected on the direction normal to the microcrack. In this manner, the stress field of the aforementioned far field based on two-dimensional Westergaard's solution can be shown[17] to lead to the expression:

$$\Lambda(\mathbf{x}, \xi) = -\frac{k(r)}{2}[\cos 2\theta + \cos 2\psi + \cos 2(\theta + \psi)] \tag{14}$$

Here θ and ψ denote the angles of the normals of the source and target microcracks at ξ and $\mathbf{x}$ with the ray connecting the centres of these microcracks (see Figure 2). A similar expression could be derived for three dimensions using the far field based on Fabrikant's solution, formulated in Reference 17.

The size of the averaging volume in which the weight function α has non-zero or non-negligible values is controlled by the average microcrack length κl. Since this length is taken to be approximately equal to the maximum aggregate size ($\kappa l = d_a$), the averaging volume at each microcrack may be, for two-dimensional problems, defined as a rectangle whose longer size is $4\kappa l = 4d_a$ (in the microcrack direction) and shorter side is $2\kappa l = 2d_a$ (in the normal direction; see Figure 3). For three-dimensional problems, the averaging volume is defined as a cylinder of radius $2\kappa l = 2d_a$ and length $2\kappa l = 2d_a$, with the axis normal to the microcrack plane.

In the present implementation, the microcrack orientations are calculated in the first iteration of each loading step and are kept constant during the subsequent iterations even though the direction of the maximum total principal strain in general changes during the iterations. This simplification seems acceptable because, according to numerical experience, the total principal strain directions do not change significantly from one iteration to the next, in the same loading step.

4. SOLUTION STRATEGIES

To calculate the nonlocal inelastic stress increments, a system of N linear equations with N unknown values of $\Delta\bar{S}_\mu^{(1)}$ must be solved [equation (5)]. This can be done either analytically or numerically, by iterations. Due to symmetry and physical meaning of the crack influence function, Gauss–Seidel iterative solution process ought to converge and may, therefore, be used to solve these unknowns.[17] If subscript r refers to the current iteration, then the approximation in the $(r + 1)$st iteration of the loading step is obtained as[17]

$$\Delta\bar{S}_\mu^{(1)[r+1]} = \langle \Delta S_\mu^{(1)} \rangle + \sum_{\nu=1}^{N} \Lambda'_{\mu\nu} \Delta\bar{S}_\nu^{(1)[r]} \Delta V_\nu \quad (\mu = 1, 2, \ldots, N) \tag{15}$$

with $\Lambda'_{\mu\nu} =$ matrix of the adjusted crack influence function.

For points near the boundaries in a finite body, the precise expression for function $\Lambda(\mathbf{x}, \xi)$ is not yet known. As a simple approximation, we will use the same function $\Lambda(\mathbf{x}, \xi)$ as for an infinite body. But one correction to this function must be introduced. For the case of homogeneous deformation of a homogeneous body, nonlocality must disappear, i.e. $\Delta\bar{S}^{(1)}(\mathbf{x}) = \langle \Delta S^{(1)}(\mathbf{x}) \rangle = \Delta S^{(1)}(\mathbf{x})$ must satisfy equation (4). Substituting this into (4) we get the condition[17] $\int_V \Lambda(\mathbf{x}, \xi)\, dV(\xi) = 0$. Thus the matrix form of the crack influence functions must be adjusted so as to satisfy the condition $\sum_{\nu=1}^{N} \Lambda'_{\mu\nu} = 0$. Because this condition may be written as $\sum_{\text{interior}} \Lambda_{\mu\nu} +$

$k_b \sum_{\text{boundary}} \Lambda_{\mu\nu} = 0$, the following adjustment is needed for the integration points of the elements adjoining the boundary:[17]

$$\Lambda'_{\mu\nu} = k_b \Lambda_{\mu\nu}; \quad k_b = -\sum_{\text{interior } \nu} \Lambda_{\mu\nu} \Big/ \sum_{\text{boundary } \nu} \Lambda_{\mu\nu} \tag{16}$$

For the integration points of the remaining elements in the interior, no adjustment is done.

The foregoing correction of $\Lambda_{\mu\nu}$ values is of course empirical. Neither analytical solutions nor test data exist to check it. In view of this fact, an even simpler procedure, replacing equation (16), has been used in all the computations reported here: The weighted sum of all $\Lambda_{\mu\nu}$ values (weighted by ΔV_ν) corresponding to each point μ was checked continuously. Whenever its magnitude exceeded a certain very small tolerance, the sum with $\Lambda'_{\mu\nu}$ was simply deleted from equation (15), which means that only the spatial (local) averaging was performed.

The average local inelastic stress increment normal to the microcrack is calculated as

$$\langle \Delta S_\mu^{(1)} \rangle = \frac{1}{V_\mu} \sum_{\nu=1}^{n} \Delta S_\nu^{(1)} \alpha_{\mu\nu} \Delta V_\nu \tag{17}$$

where $V_\mu = \sum_{\nu=1}^{n} \alpha_{\mu\nu} \Delta V_\nu$ (normalizing volume) and n = total number of integration points within the region in which the values of the weight function $\alpha_{\mu\nu}$ are non-zero and non-negligible. Same as for the preceding sum, the integration points are considered to contribute to this sum only when the stress increments for both μ and ν are positive. The weight function is implemented in the form of a bell-shaped function (4th degree polynomial, Reference 13). It equals unity at the microcrack centre and attains zero at the boundary of the averaging region (rectangle or prism).

Each Gauss–Seidel iteration is initialized by setting the nonlocal stress increments $\Delta \bar{S}_\mu^{(1)}$ to be equal to the local inelastic stress increments $\Delta S_\mu^{(1)}$ obtained from the constitutive law, which is strictly local (as it characterizes the behaviour of a homogeneously deforming material element). The values of $\Delta \bar{S}_\mu^{(1)}$ are progressively updated during the iterations. The solution converges when the maximum stress difference between the current and the previous iteration becomes less that the prescribed tolerance on the relative stress changes. From experience, the convergence of iterations is good.

The foregoing iterative procedure, however, causes slight non-symmetry of the response in the structural softening regime even when the structure is symmetric. The reason is that the integration points from one side of the symmetry axis have already been updated when the nonlocal stress increments at the symmetric point on the other side of the symmetry axis are being calculated. Nevertheless, this non-symmetry can be made as small as desired by prescribing a small enough tolerance for termination of the iterations.

Efficiency of the Gauss–Seidel iterative procedure also depends on which solution strategy is used at the level of each loading step, for example, the constant initial stiffness matrix method or the tangent stiffness method. Strictly speaking, the foregoing formulation calls for using in each loading step separate Gauss–Seidel iteration procedures, one for the local nonlinear constitutive law (to calculate the local inelastic stress increments), and another for the crack interactions (to calculate the nonlocal inelastic stress increments). However, as suggested in Bažant,[17] both iterations may be combined into one iteration loop. Experience with this approach, which is more efficient and simpler to program, indicates that it normally converges satisfactorily.

Note that the Gauss–Seidel iteration procedure for solving the system (5) is analogous to the relaxation method known from the analysis of frame structures, in particular the Cross method or moment distributions method.

On the global solution level of the present numerical implementation, the total stress tensor is updated after each iteration rather than only after each loading step. Experience from the present numerical studies indicates no significant dependence on the loading path. Of course, the degree of path dependence is also related to the choice of the local constitutive model. In principle, any constitutive model that is able to handle post-peak material softening may be combined with the present approach to nonlocality due to microcrack interactions. So far, however, broad experience exists only for the recently improved microplane constitutive model for concrete.[13,25-27] A very effective new microplane model with stress–strain boundaries[7] could also be used. Note, however, that the path dependence could be stronger for plasticity models. In that case it might be better to use a solution strategy in which the total stress tensor is updated only after each loading step.

5. IDENTIFICATION OF NONLOCAL MATERIAL MODEL PARAMETERS

The main difficulty in using the present model lies in identifying the material parameters of the nonlocal material model according to the given basic macroscopic properties of concrete. A theoretically rigorous and accurate closed-form solution to this problem is not only unavailable but also hardly feasible. However, based on the physical meaning of the present nonlocal concept, an approximate procedure can be formulated. It transpires that: (1) the uniaxial tensile strength is mainly controlled by the tensile strength f_t' for the local constitutive model, and (2) the macroscopic fracture energy G_f is mainly controlled by the maximum aggregate size d_a (which is roughly proportional to the dominant microcrack spacing) and to the area under the local stress–strain curve for direct tension (Figure 5). The following procedure has been found to give good results.

As already mentioned, the characteristic length for the nonlocal interactions may be approximately given by

$$\kappa l = d_a \tag{18}$$

because the size and spacing of the dominant microcracks must be roughly proportional to d_a. Then one needs to estimate G_f and f_t'. Since the tensile resistance depends on size and shape, one must take into account the size effect, which at the same time offers the easiest approach for determining G_f. Thus, one may conveniently apply the size effect law proposed by Bažant[18] to the analysis of maximum loads P_u of geometrically similar fracture specimens of different sizes, using a procedure based on fitting the maximum load values with the size effect law.[28] The extrapolation

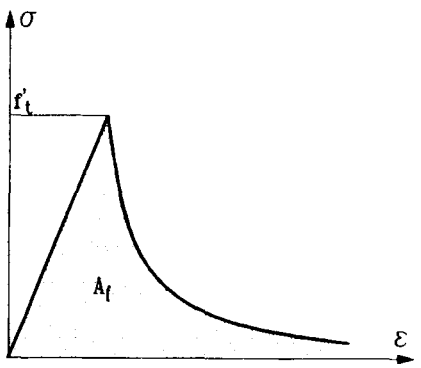

Figure 5. Simple and realistic tensile local stress–strain curve for concrete (f_t' and A_f are the input parameters and the curve is exponential)

to very large size yields the approximate values of fracture energy G_f. The material tensile strength can be approximately obtained as $f_t' = P_u/A_c$ where A_c = cross-section area of concrete in the critical cross-section and P_u = failure load at crack initiation (approximately homogeneous uniaxial tensile stress–strain field).

For the estimation of strain-softening, consider the approximate relation $abG_f = abw_c A_f$ where a, b = crack length and width (ab = crack surface area), w_c = effective width of the crack band at the fracture front (abw_c = volume traversed by the advancing crack band front), and A_f = complete area under the local stress–strain diagram (Figure 5), which represents the energy dissipated per unit volume (cracking energy density). Again, w_c obviously ought to be proportional to d_a. Empirically, it has been found that the value $w_c = 8d_a$ gives good results, which means that

$$A_f = G_f/8d_a \tag{19}$$

The ratio of w_c to d_a may seem much too large. But it does not seem so if one realizes that on the microscale the fracturing localizes mainly in the zones of near contact between aggregate pieces, while the local stress–strain relation describes the fracturing deformations in a smeared way. Knowing A_f, one can correctly choose the mean downward post-peak slope of the local uniaxial tensile stress–strain diagram (Figure 5).

Before equation (19) can be applied, the shape of the local stress–strain diagram must be selected. A good and simple approximation is the exponential shape (e.g. Reference 29, Figure 5), which was adopted for the present calculations. This shape may have considerable influence on some types of structural response.

The foregoing procedure allows simple albeit crude calibration of the material model. It applies not only to tension (or mode I) dominated failures, but also to shear (or modes II and III) dominated failures, provided the shear failure microscopically develops through mode I microcracks inclined with respect to the direction of shear (as demonstrated already in Reference 30).

Nonlocal finite element calculations of notched fracture specimens according to the present method have been carried out to check whether the tensile strength and fracture energy values obtained from the microplane model with crack interactions are about the same as their initial estimates according to the foregoing procedure. The specimen geometry, boundary conditions and finite element discretization are shown in Figure 6. The specimen was loaded by controlling

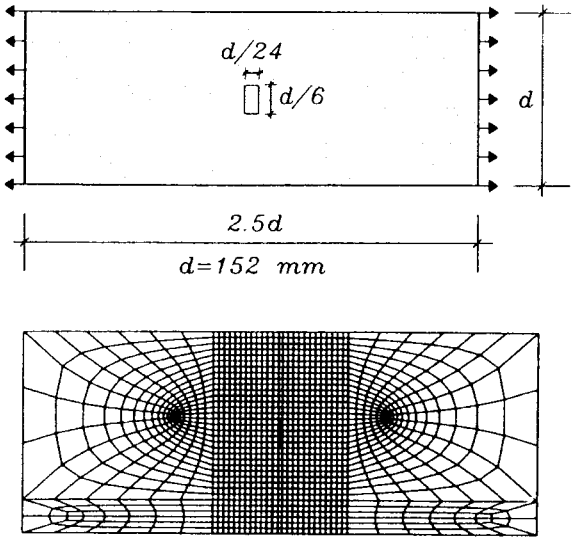

Figure 6. Uniaxial tensile specimen and finite element mesh used to check the calibration procedure of the model

the horizontal displacement at the vertical edges. The plane strain analysis was carried out using the microplane material model with linear pre-peak stress–strain curve on each microplane and an exponential curve for tensile post-peak softening.[29] The specimen thickness was adjusted so as to avoid snapback instability of the response, and was taken as $b = 38$ mm. The maximum size of the finite elements was approximately 3 mm. The properties of concrete were taken as follows: Young's modulus $E = 27000$ MPa, Poisson ratio $\nu = 0{\cdot}18$ and tensile strength $f_t' = 2{\cdot}5$ MPa. In the analysis, three different maximum aggregate sizes were considered ($d_a = 4$, 8 and 12 mm). The corresponding fracture energies were estimated from experimental evidence[31] as $G_{f,d_a=4} = 0{\cdot}05$ N/mm, $G_{f,d_a=8} = 0{\cdot}08$ N/mm, $G_{f,d_a=12} = 0{\cdot}10$ N/mm. The corresponding local tensile stress–strain curves used in the analysis are shown in Figure 7.

The calculated nominal stress-crack opening curves are plotted in Figure 8 for all the three cases. The resulting tensile strength is calculated as the peak load divided by the net cross-section area. The fracture energy is calculated from the area under the resulting stress-crack opening curve. Note, however, that this method of calculating fracture energy is only approximate, for reasons mentioned above and other well-known reasons.

The estimated input and the resulting values of the basic material parameters are summarized in the table in Figure 8. As can be seen, the calculated tensile strengths are for all the three cases approximately the same and equal to $f_t' = 3{\cdot}0$ MPa. These values are slightly larger than the input tensile strength ($f_t' = 2{\cdot}5$ MPa). The reason for this is the size effect caused by cracking. The table in Figure 8 demonstrates that the input value of fracture energy estimated using (19) is indeed a relatively good approximation of the fracture energy value actually calculated from the nonlocal microplane model with crack interactions. The error is approximately 20 per cent. For smaller aggregate sizes, the input values underestimate, and for larger sizes, overestimate, the actual value for the model. The reason for this probably is that, in all our examples, the size of the finite elements in the mesh has been kept constant, which caused that for larger aggregate sizes the description of the strain field was 'more smooth' than for smaller aggregate sizes.

The calculated crack-opening curves are compared in Figure 9 with the experimentally measured (average) results ($d_a = 2$ and 16 mm,[31]). As we can see, the calculated critical crack openings w_c show qualitatively the same trend as in the experiments, i.e., for larger aggregate sizes

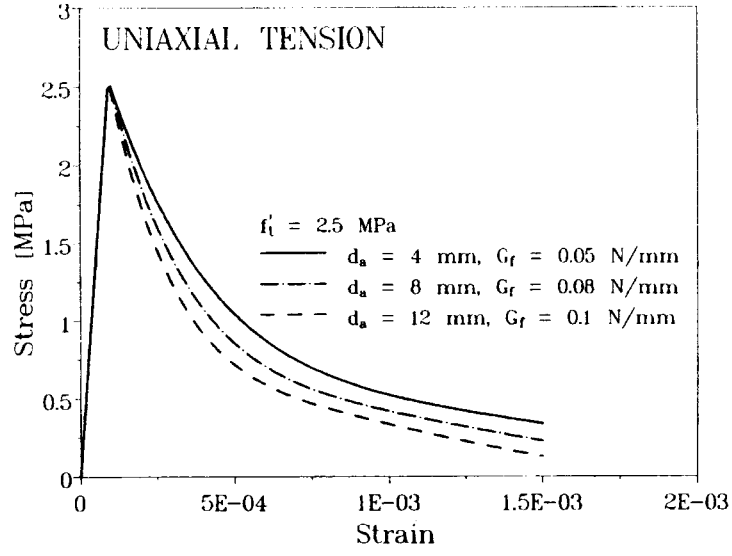

Figure 7. Three different local tensile stress–strain curve corresponding to three different aggregate sizes and fracture energies

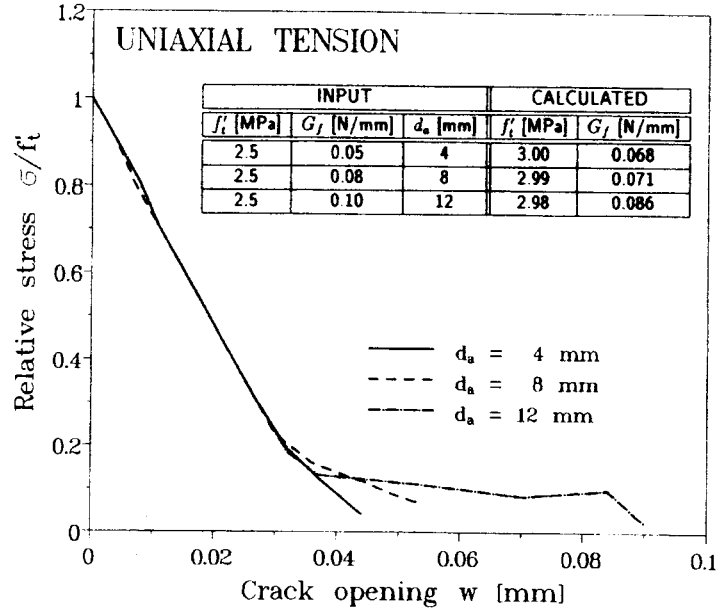

Figure 8. Calculated nominal stress-crack opening curve for three different aggregate sizes

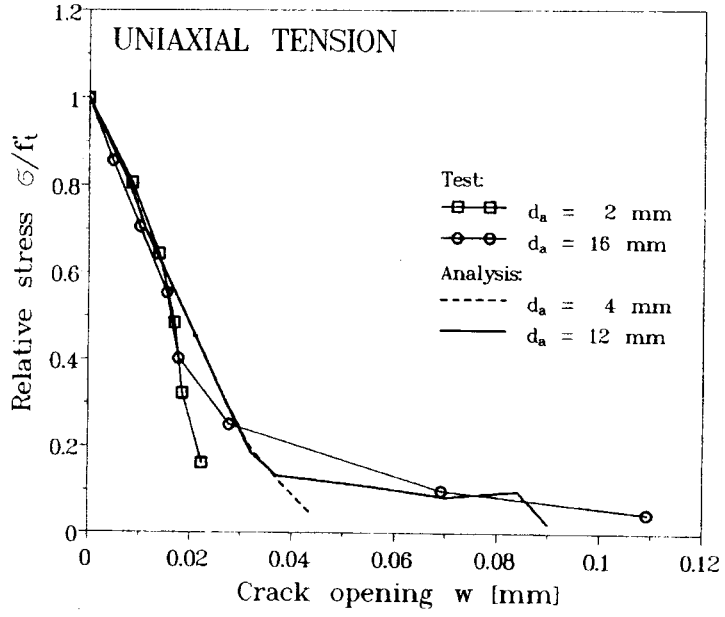

Figure 9. Comparison between calculated and experimentally measured average stress-crack opening curves for two different aggregate sizes (micro-concrete and normal concrete)

the stress-crack opening curve is more ductile. The shape of the calculated crack opening curves for micro-concrete ($d_a = 4$ mm) is practically a straight line, without any ductility before the failure. However, for a large aggregate size ($d_a = 12$ mm), pronounced ductility before failure may be observed.

The aforementioned procedure for calculating G_f can be used only under the condition that the finite element size L_e in the fracture process zone is not larger than the maximum aggregate size. This is the upper limit for L_e. For $L_e \gg d_a = l$, the nonlocal analysis becomes equivalent to the

crack band approach. However, this is inevitable in practical analyses of large structures (or in size effect studies). To handle such cases, Bažant[32] proposed to increase the characteristic length l such that it becomes at least the same or larger than the element size, i.e., $l = d_a^* \geqslant L_e$ with $d_a^* =$ equivalent aggregate size. But, in order to compensate for the effect on fracture energy (under the assumption that damage does not remain uniform), one must at the same time replace the crack energy density (A_f) with a modified value, A_f^*, so as to keep G_f constant. Therefore, according to (19),

$$G_f = 8 d_a A_f = 8 d_a^* A_f^* \tag{20}$$

and

$$A_f^* = \frac{G_f}{d_a^*} \tag{21}$$

In (21), A_f^* must be calculated keeping constant both the hardening part of the stress–strain curve and the local concrete tensile strength. Only the softening part of the local stress–strain curve must be adjusted. If this modification is not possible, the mesh with $L_e \gg d_a$ cannot be used and must be refined. However, in practice there exist problems that are insensitive to the tensile strength, as the structural response is mainly controlled by G_f. For such a case, beside the hardening part of the tensile local stress–strain curve the local tensile strength may be also modified. (Note that the softening part of the local tensile stress–strain curve must always exist since otherwise continuum fracture analysis based on the microcrack interaction approach would make no sense.)

To illustrate the procedure when $L_e > d_a$, the aforementioned test specimen has been analyzed using the following input values for concrete properties: $f_t' = 2{\cdot}5$ MPa, $G_f = 0{\cdot}08$ N/mm and $d_a = 8$ mm, with all the other parameters the same as in the preceding example. Let us now consider two different characteristic lengths: the actual one, $l = d_a = 8$ mm, and the modified one, $l = d_a^* = 12$ mm. For the original value $l = d_a = 8$ mm, A_f is calculated using (19). To keep G_f constant when the characteristic length is changed, the cracking energy density A_f for $l = 12$

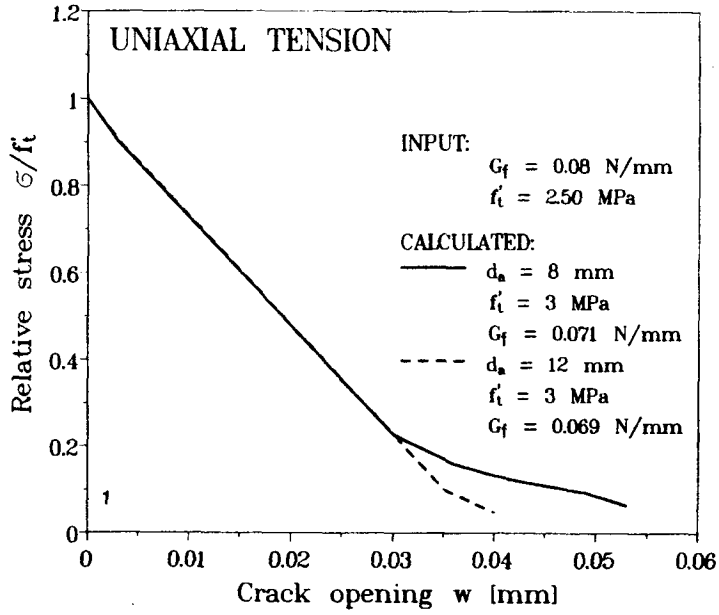

Figure 10. Stress-crack opening curves calculated when concrete properties correspond to different characteristic lengths

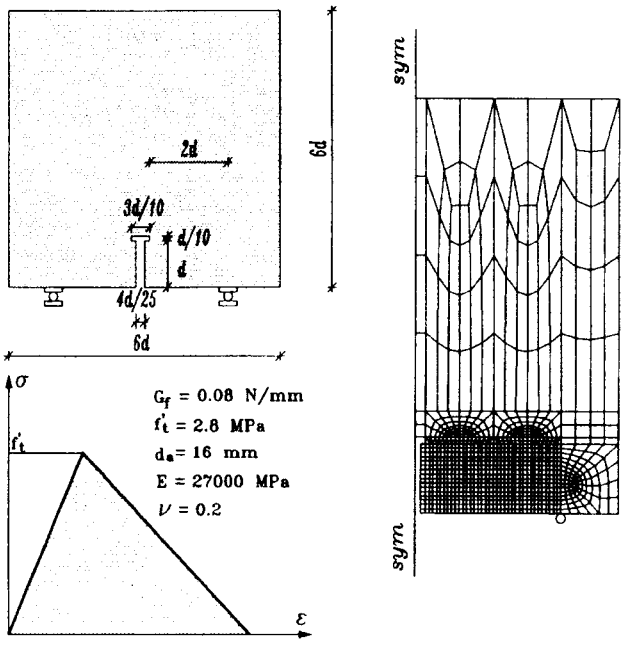

Figure 11. Geometry, typical finite element mesh, and material properties used in calculation of pull-out of headed stud to check the calibration procedure

mm must be modified according to (21). The calculated stress-crack opening curves for both cases are plotted in Figure 10. As we can see, the response as well as the calculated G_f values for $l = d_a^* = 12$ mm are approximately the same as for the actual value of $l = d_a = 8$ mm.

Another example is simulation of the pull-out of a headed stud from a plain concrete block. The analysis is carried out using axisymmetric finite elements and the microplane constitutive model for concrete. The geometry, material properties and typical mesh are given in Figure 11. The maximum aggregate size is $d_a = 16$ mm. The bar embedment depth is $d = 1350$ mm. For such a large structure it is not possible to use finite element size $L_e < d_a$ since at least 10000 finite elements would be required. Obviously, a courser mesh must be used in order to reduce the number of elements. To check the objectivity of the analysis when the discretizations are relatively coarse, two companion analyses are carried out. In the first, a relatively coarse mesh, with approximately 1400 elements, is used along with the modified value $l = d_a^* = 60$ mm. In the second, the mesh is refined to approximately 2500 elements, and the actual value $l = d_a^* = 30$ mm is used.

The calculated load-displacement curves for both examples are plotted in Figure 12. As we can see, the peak loads for both cases are practically the same (note that they are also approximately equal to the peak load calculated from Eligehausen and Sawade's[33] empirical formula).

The foregoing examples confirm that calibration of the nonlocal material model parameters to match the macroscopic properties of normal concretes with reasonable accuracy is not difficult with the proposed procedure. However, beside the aforementioned lower limit for the characteristic length ($l > L_e$), an upper limit also exists. Namely, due to the smeared cracking concept, it turns out and experience confirms that the characteristic length must be $l < D/10$, with D = characteristic dimension (size) of the structure (e.g., the beam depth, embedment depth, etc.). Otherwise, for the crack influence function based on the stress field of a crack in infinite solid, the microcrack interaction becomes meaningless because the influence of boundaries becomes too strong and condition (6) cannot be fulfilled. Thus, for small structures, it may happen that l must

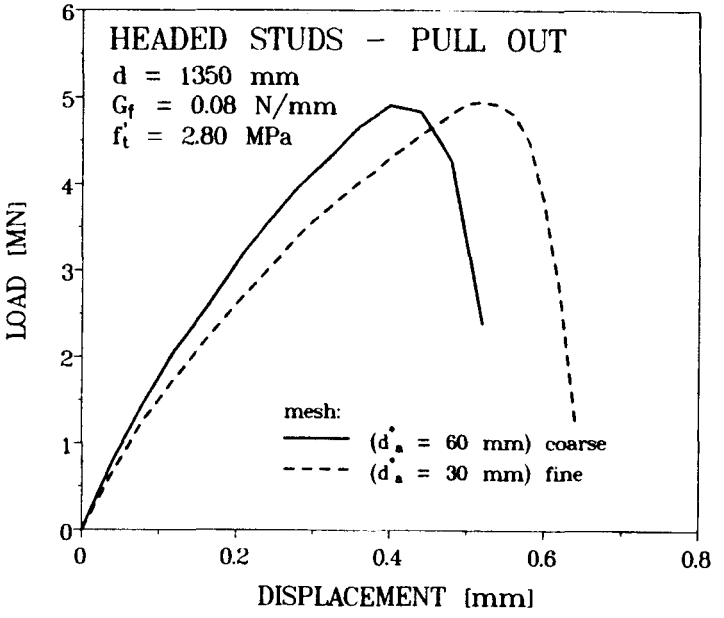

Figure 12. Calculated pull-out load–displacement curve for two different meshes—fine and coarse

be set smaller then d_a, as indicated by the present approximate calibration procedure. However, this procedure may generally lead to an excessively ductile local tensile stress–strain curve, which may influence the results unrealistically. For instance, it may prevent localization of damage and completely change the failure mechanism. To avoid such problems for $l < d_a$, the local tensile stress–strain curve must be modified by introducing into it a short horizontal plateau or, alternatively, by increasing the local tensile strength, provided that, of course, one deals with a response that is insensitive to tensile strength.

The choice of the finite element type is also important for the present approach. Generally, higher-order elements are more effective since the same strain field can be represented with a smaller number of elements equally well. When higher-order elements are used, the size of the elements does not need to be smaller than $d_a/2$. Namely, fracture energy is consumed in a finite volume of concrete (rather than zero volume—a line or surface), which is proportional to the maximum aggregate size d_a. Therefore, when the structure is so small that the characteristic length must be less than d_a (due to boundary influence), the local tensile stress–strain curve may be too ductile and make the analysis unobjective. This is always a problem in the crack band approach because for that approach the local tensile stress–strain curve is related only to the element size, instead of the maximum aggregate size and the stress and strain fields. This is what in general leads to excessive mesh sensitivity. Thus, in the present approach, the optimal choice for the given macroscopic concrete properties (f'_t, G_f) is to relate both the material model parameters and the size of finite elements to the maximum aggregate size.

6. NUMERICAL STUDIES

6.1. Influence of microcrack interaction

To demonstrate the influence of microcrack interactions, the tensile specimen shown in Figure 6 is analysed with and without the contribution of microcrack interaction (i.e. using only local

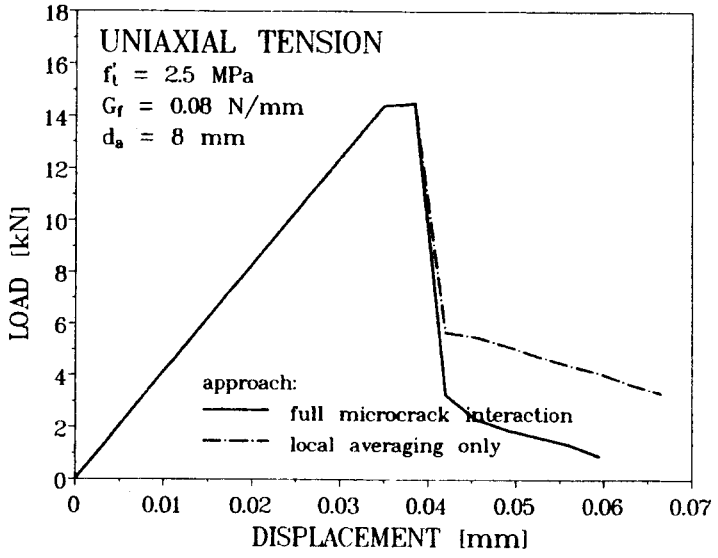

Figure 13. Calculated load–displacement curves of the tensile specimen from Figure 6, with and without microcrack interaction

averaging in the latter case). The geometry of the specimen and the material properties are the same as used for the previous example with Figure 6, i.e. $d_a = 8$ mm and $G_f = 0{\cdot}08$ N/mm.

The calculated load–displacement curves are plotted in Figure 13. For both cases, the same peak load is obtained, however, the softening curve calculated without microcrack interactions exhibits a more ductile response. The reason is that the crack influence function correctly releases the stresses (i.e., reduces them to zero) when the microcrack system tends to coalesce into a single macrocrack. Note that a similar result has been obtained theoretically by Pijaudier-Cabot and Berthaud.[34]

6.2. *Mesh sensitivity study*

As already mentioned, an important requirement for continuum smeared cracking analysis is that the results must be independent of the mesh size and geometry, especially the orientation. To check it, a simple specimen, loaded in eccentric tension, is analysed up to failure under the assumption of plane strain, using four different finite element discretizations. The geometry of the specimen, finite element meshes and material model properties are shown in Figure 14. The

a)

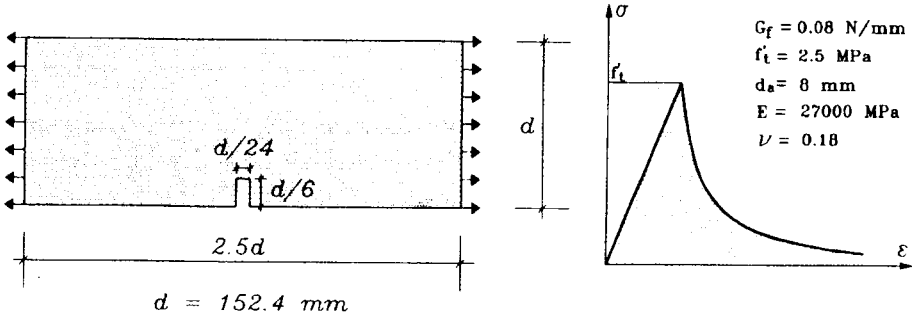

Figure 14. (a).

b)

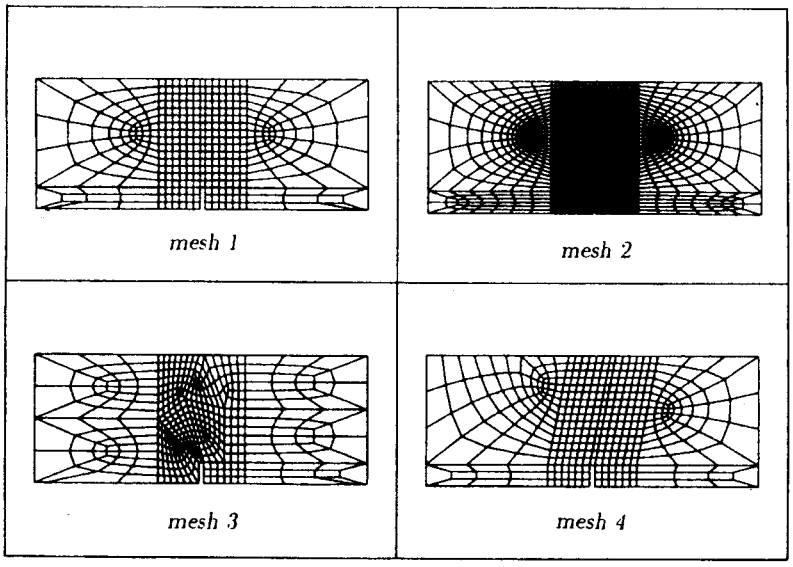

Figure 14. Geometry of single-edge-notched tensile fracture specimen, material properties, and four different FE meshes used in mesh sensitivity study

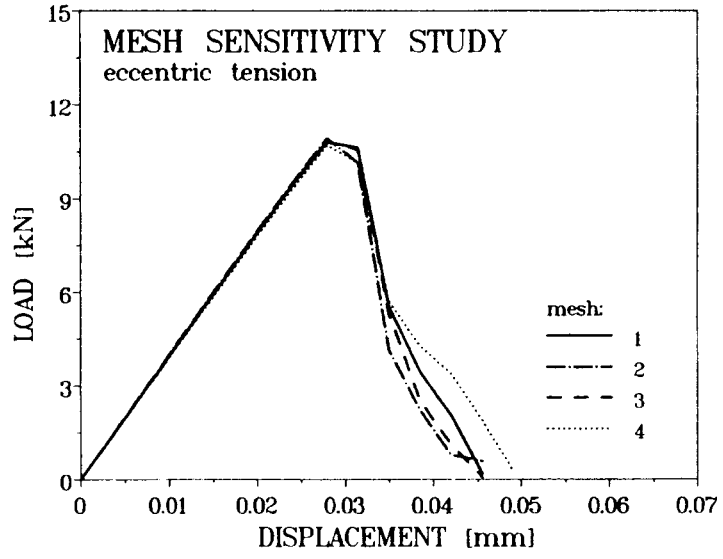

Figure 15. Calculated load-crack opening curves for four different finite element discretizations

calculated load–displacement curves for all the four cases are plotted and compared in Figure 15. As can be seen, no significant differences in the resulting load–displacement curves can be observed for the four different meshes. Objectivity of the analysis is also confirmed by Figure 16 where the final damage zones at the end of loading are seen for two different meshes. The dark zone in Figure 16, which represents the zone where the strains are increasing near the end of the analysis, indicates localization of damage. Regardless of the mesh configuration, the damage is seen to be localized into a band of approximately constant width which is related to the

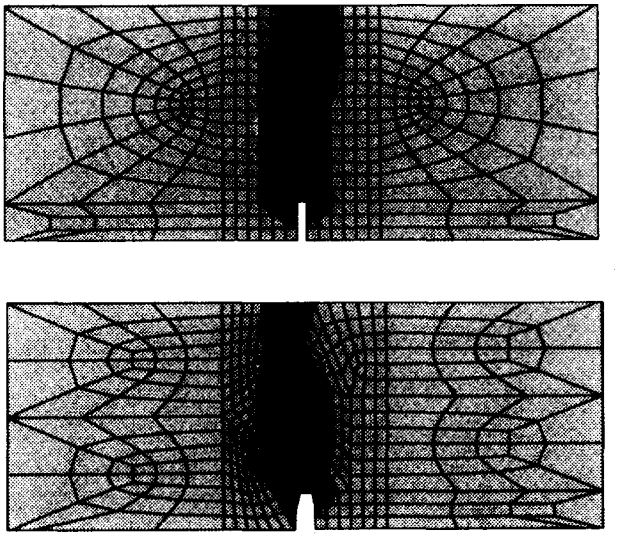

Figure 16. Crack patterns at termination of analysis for mesh 1 and mesh 3

characteristic length (maximum aggregate size). This means that the energy consumed by fracture is approximately the same and independent of the mesh.

6.3. *Size effect studies for prototype problems*

In the microcrack interaction approach, the effective characteristic length, expressed in the sense of the nonlocal strain approach, depends on the stress and strain fields and is changing during the analysis. As already discussed, heterogeneity of concrete strongly depends on the aggregate size and shape. It seems reasonable to assume the microcrack length to be proportional to the maximum aggregate size which, together with the stress and strain fields, controls the reach of microcrack interaction. To check whether such approach can correctly predict failure for different problems using only macroscopic concrete properties (f_t', G_t and d_a) as the input data, the size effect studies for prototype problems, such as uniaxial tension, three-point bending, eccentric compression, diagonal shear and pull-out of headed studs, have been carried out and compared with the available experimental evidence.

Furthermore, geometrically identical specimens under different loads, shown in Figures 17(a)–17(d) and 11, are analysed using the microplane model as the constitutive law for continuum damage, with the material properties indicated in the figures. The experimentally obtained and calculated peak loads for all the specimens are plotted and compared in Figure 18(a)–18(e). In the same figures, the calculated results are also compared with the size effect law,[18] which has been extensively validated before. This law is seen to fit the test data for the present size ranges quite well. The calculated peak loads are seen to be in good agreement with the experimental evidence. To illustrate the power of the present approach and the objectivity of the smeared fracture analysis, the typical failure modes of reinforced concrete beams and pull-out specimens are revealed by the shapes of the damage zones at different loading stages in Figures 19 and 20.

The foregoing numerical results confirm that the present microcrack interaction approach is able to correctly predict failure for the basic prototype problems using only standard, usually known, macroscopic concrete fracture properties. This is the main practical advantage of the

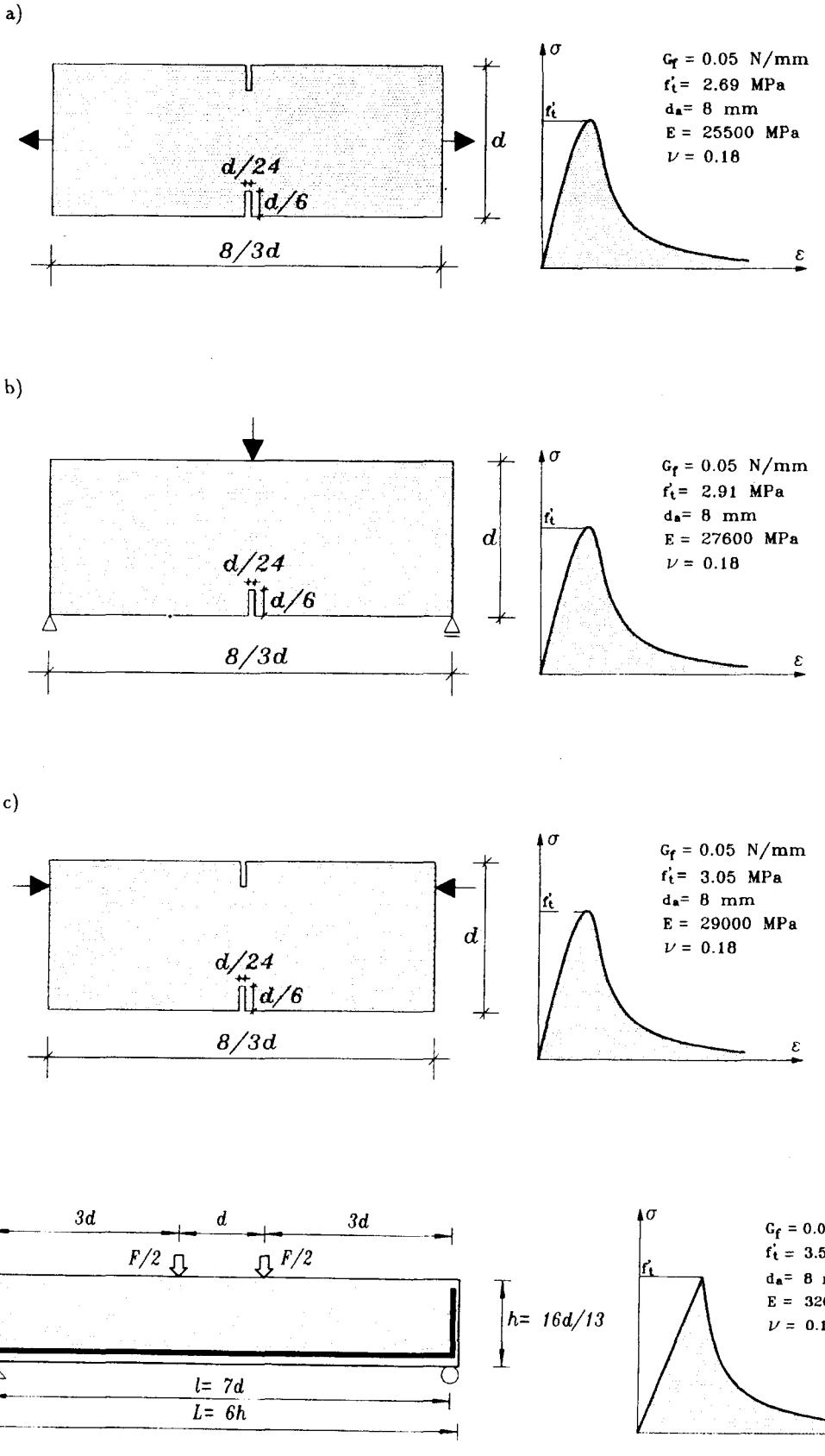

Figure 17. Size effect study: geometry of specimens and material properties for different problems; (a) uniaxial tension, (b) three-point bending, (c) eccentric compression and (d) diagonal shear of RC beams without shear reinforcement

a)

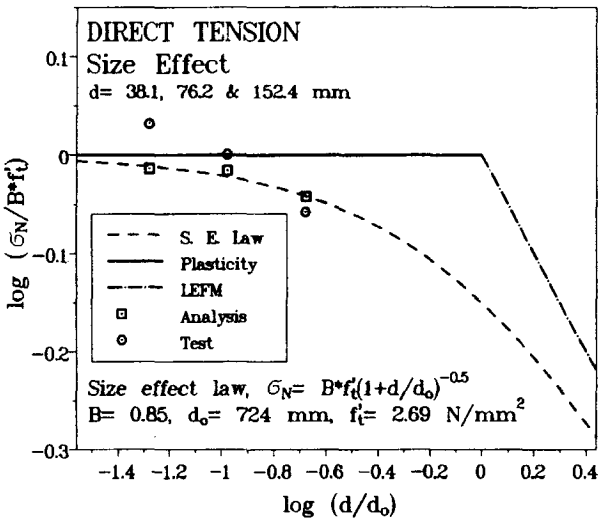

b)

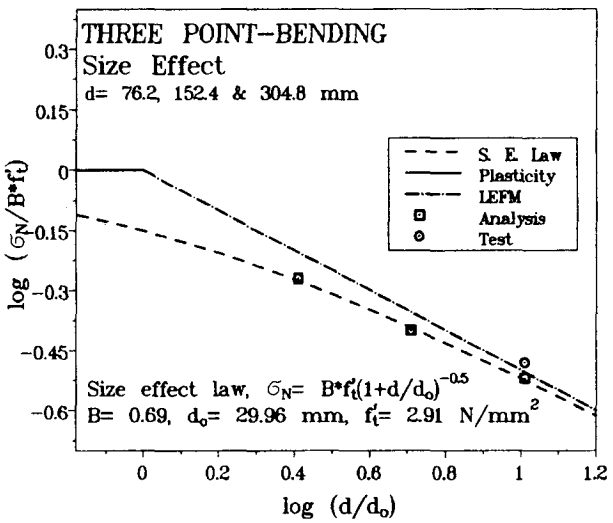

c)

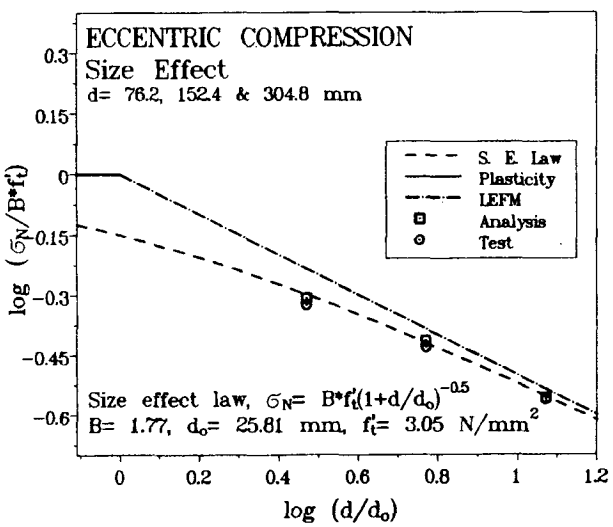

Figure 18. (a–c)

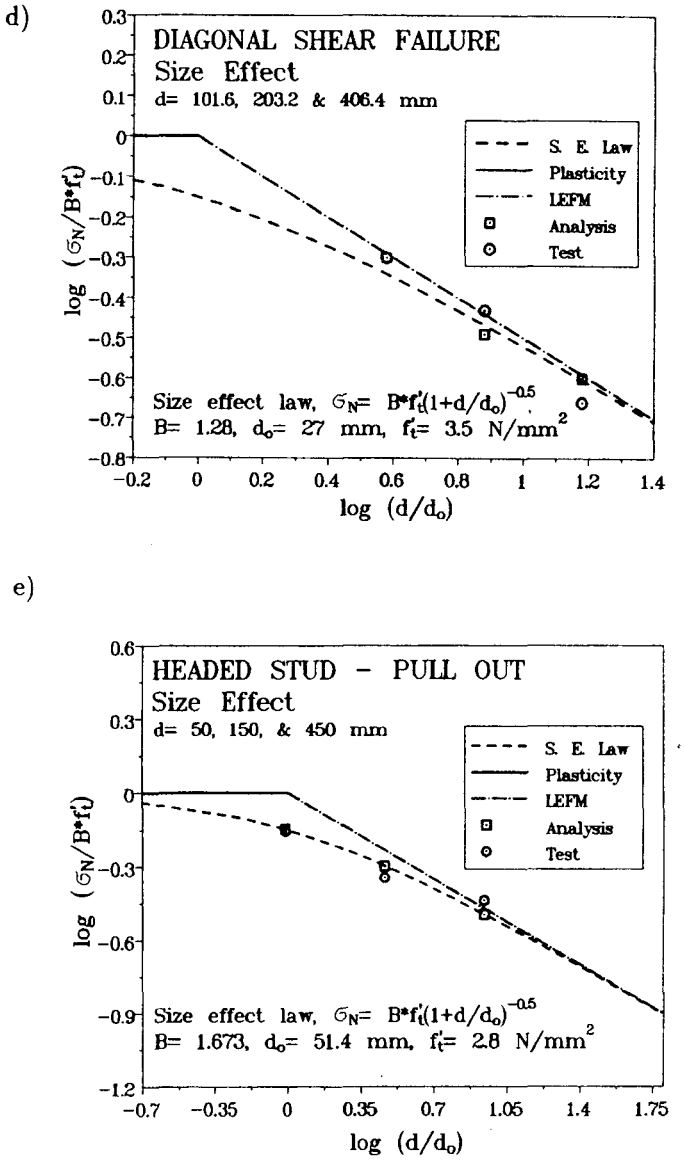

Figure 18. Calculated failure loads for different sizes compared with test results and Bažant's size effect law: (a) uniaxial tension, (b) three-point bending, (c) eccentric compression, (d) diagonal shear, and (e) pull-out of headed stud. For each problem type the constants B and d_0, for plotted size effect curves, are obtained by the linear regression analysis of calculated data

nonlocal microcrack interaction approach over other the previous nonlocal approaches, in which different material properties had to be used for different types of problems.

7. CONCLUSIONS

1. Nonlocality is not merely an expedient mathematical device serving as a localization limiter in smeared fracture analysis. The new nonlocal microcrack interaction approach has its physical origin in the interaction of growing microcracks. In this new nonlocal approach, one must distinguish two kinds of spatial integrals: (1) the local averaging and (2) the long-range interaction. The former defines the volume in which energy consumption by

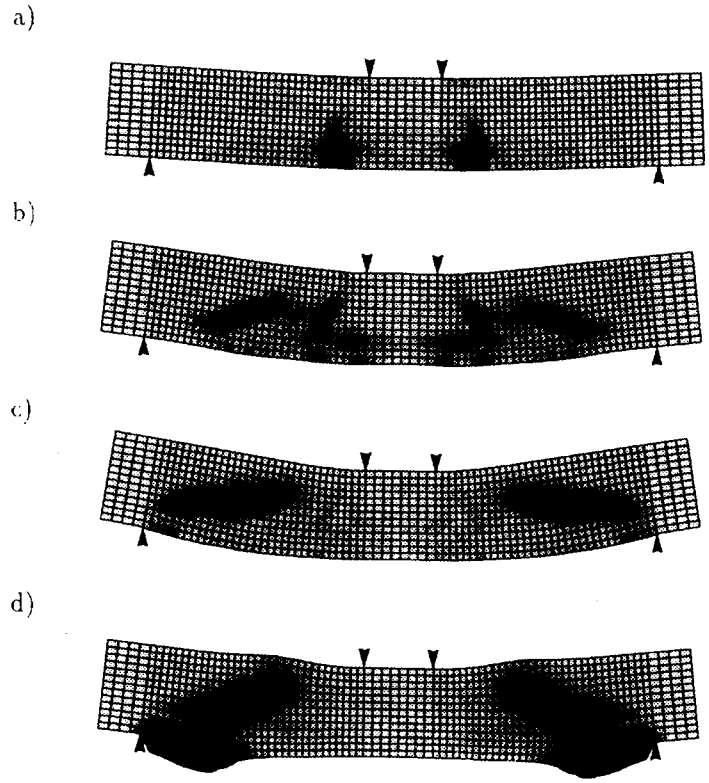

Figure 19. Crack pattern (traced from principal strains) for RC beam without shear reinforcement ($h = 100$ mm) at different loading stages; (a) initiation of bending cracks, (b) 75 per cent of peak load, (c) peak load and (d) termination of the analysis (displacement factor = 50)

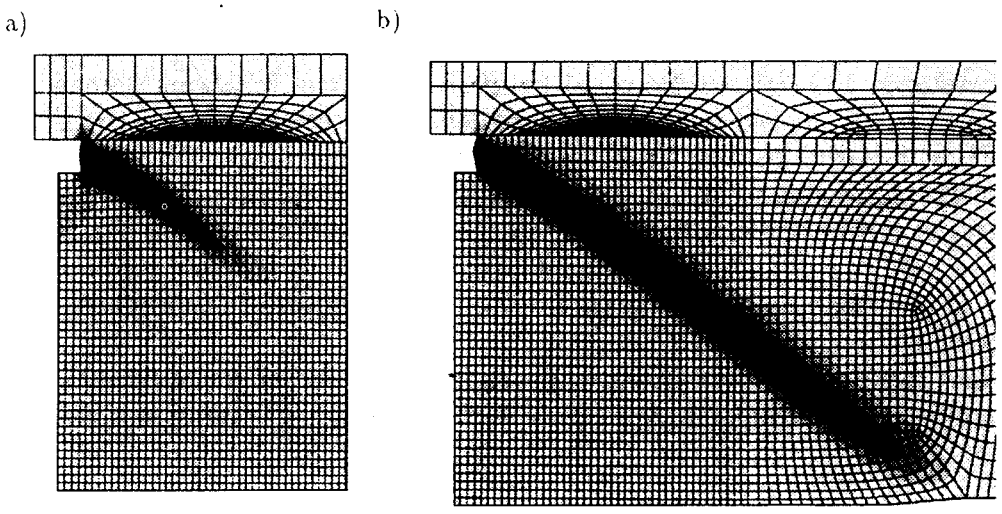

Figure 20. Crack pattern for pull-out of headed stud from a concrete block with embedment depth $d = 900$ mm; (a) peak load and (b) termination of the analysis

fracture takes place. The latter controls crack opening and propagation as a function of the stress and strain fields in the neighbourhood of a microcrack and, which is practically most important, it achieves correct (mesh-independent) energy release and reduction of stresses to zero when the system of microcracks coalesces into a single macrocrack.

2. As numerical examples show, the new approach ensures damage to localize into a material volume whose size and shape are independent of the shape and size of the finite elements.

According to arguments of concrete heterogeneity and randomness of microcrack distribution, the size of the domain of nonlocal integrals is a function of the current stress–strain state and the typical dominant microcrack length (approximately equal to the maximum aggregate size).

3. It is demonstrated that the nonlocal material model parameters can be approximately correlated to the given macroscopic concrete properties (tensile strength, fracture energy and maximum aggregate size). These input parameters may then be used in fracture analysis of different problems with no need for their calibration according to the problem type. Together with a realistic local material model for concrete, the new approach is thus able to predict more complicated failure modes (including modes II and III) automatically (as long as Mode II and III fractures consist of a band of inclined Mode I microcracks).
4. The best results in fracture analysis are obtained if both the material model parameters and the finite element sizes are related to the maximum aggregate size. The reason is that the energy is consumed by concrete fracture in a finite material volume (rather than in a line or surface of zero volume). The size of this volume may be approximately related to the maximum aggregate size. The local type of smeared crack band analysis, even with extremely fine meshes, generally leads to mesh dependence unless the mesh lines are laid in the correct crack propagation direction. The crack band model is objective only when the mesh line coincides with the fracture path.
5. In the finite element implementation, the nonlocal inelastic stress increments are calculated from the known tensile local stress–strain curve using the superposition principle and the Gauss–Seidel iterative procedure. The concept is independent of the non-linear triaxial constitutive model, which is local. Any model for strain-softening may be used. So far, broad experience exists only with the microplane constitutive model. Further studies are required to determine the influence of various solution strategies and constitutive models when the new nonlocal concept is used.
6. The results of analysis are shown to be mesh insensitive. Cracking damage is found to localize into a volume whose size and shape depend on the macroscopic concrete properties as well as the current stress–strain state.
7. Although microscopically the damage is treated as tensile, being caused by mode I microcracks, the experience with the new nonlocal approach indicates that it can also describe quite well the complex shear-dominated mixed-mode types of failure, and can do so for the same values of material parameters as for Mode I failures (which has not been achieved with the previous nonlocal models).
8. The new nonlocal model can correctly capture the size effect of fracture and damage mechanics, in approximate agreement with the size effect law proposed by Bažant.[18]

ACKNOWLEDGEMENT

Partial financial supports from Stuttgart University and from AFOSR (under Grant 91-0140 to Northwestern University) are gratefully acknowledged.

REFERENCES

1. Z. P. Bažant, 'Imbricate continuum and progressive fracturing of concrete and geomaterials', *Meccanica* (Italy) (Special issue commemorating the centennial of A. Castigliano's death), **19,** 86–93 (1984).
2. Z. P. Bažant and B. H. Oh, 'Crack band theory for fracture of concrete', *Materials and Structures* (RILEM, Paris) **16** (93), 155–177 (1983).

3. J. G. Rots, 'Computational modeling of concrete structures', *Doctoral Dissertation*, Delft, The Netherlands, 1988.
4. R. de Borst and J. G. Rots, 'Occurrence of Spurious Mechanisms in Computations of Strain Softening Solids', *Eng. Comput.*, **6**, 272–280 (1989).
5. R. de Borst, 'Continuum models for discontinuous media.' *Proc. Internat. RILEM/ESIS Conf. on Fracture Processes in Concrete, Rock and Ceramics*, Noordwijk, The Netherlands, 1991, pp. 601–618.
6. J. Ožbolt and R. Eligehausen, 'Analysis of reinforced concrete beams without shear reinforcement using nonlocal microplane model,' *Proc. Internat. RILEM/ESIS Conf. on Fracture Processes in Concrete, Rock and Ceramics*, Noordwijk, The Netherlands, 1991, pp. 919–930.
7. Z. P. Bažant, Y. Xiang and P. C. Prat, 'Microplane for concrete: I. stress–strain boundaries and finite strain', ASCE *J. of Eng. Mech.*, **122**, (1996) in press.
8. A. C. Eringen, 'Theory of micropolar continuum', *Proc., Ninth Midwestern Mech. Conf.*, University of Wisconsin, Madison, 1965, pp. 23–40.
9. A. C. Eringen, 'A unified theory of thermomechanical materials', *Int. J. Eng. Sci.*, **4**, 179–202 (1966).
10. E. Kröner, 'Interrelations between various branches of continuum mechanics', in E. Kröner, (ed.), *Mechanics of Generalized Continua*, Springer, Berlin, 1968, pp. 330–340.
11. Z. P. Bažant, 'Imbricate continuum and its variational derivation', *J. Eng. Mech. ASCE*, **110**, 1693–1712 (1984).
12. G. Pijaudier-Cabot and Z. P. Bažant, 'Nonlocal damage theory', *J. Eng. Mech. ASCE*, **113**, 1512–1533 (1987).
13. Z. P. Bažant and J. Ožbolt, 'Nonlocal microplane model for fracture, damage, and size effect in structures', *ASCE J. Eng. Mech.*, **116**(11), 2484–2504 (1990).
14. J. Ožbolt, 'General microplane model for concrete', in Folker H. Wittmann (ed.), *Numerical Models in Fracture Mechanics of Concrete*, Swiss Federal Institute of Technology, Switzerland, 1993, pp. 173–187.
15. Z. P. Bažant, 'Why continuum damage is nonlocal: micromechanics arguments', *J. Eng. Mech. ASCE*, **117**, 1070–1087 (1991).
16. G. Pijaudier-Cabot and Z. P. Bažant, 'Cracks interacting with particles or fibers in composite materials', *J. Eng. Mech. ASCE*, **117**, 1611–1630 (1991).
17. Z. P. Bažant, 'Nonlocal Damage Theory Based on Micromechanics of Crack Interactions', *J. Eng. Mech. ASCE*, **120**, 593–617 (1994); with Addendum, **120**, 1401–1402.
18. Z. P. Bažant, 'Size effect in blunt fracture: concrete, rock, metal', *J. Eng. Mech. ASCE*, **110**, 518–535 (1984).
19. W. D. Collins, *Proc. Roy. Soc.* A274, **1359**, 507–526 (1963).
20. M. Kachanov, 'A simple technique of stress analysis in elastic solids with many cracks', *Int. J. Fracture*, **28**, R11–R19 (1985).
21. M. Kachanov, 'Elastic solids with many cracks: a simple method of analysis', *Int. J. Solids Struct.*, **23**, 23–43 (1987).
22. Z. P. Bažant and M. Jirásek, 'Damage nonlocality due to microcrack interactions', *Fracture and Damage in Quasibrittle Structures: Experiment, Theory and Computational Aspects* (Proc., Europe-U.S. Workshop, held in Prague, September 1994), Z. P. Bažant *et al.* (eds.), Spon, London and New York, 1994, pp. 3–17.
23. D. Broek, *Elementary Engineering Fracture Mechanics*, Martinus Nijhoff, Doordrecht-Boston, 1987, p. 77.
24. V. I. Fabrikant, 'Complete solutions to some mixed boundary value problems in elasticity, in J. Hutchinson and T. Wu (eds.), *Advances in Applied Mechanics*, Vol. 27, Academic Press, New York, 1990, pp. 153–223.
25. Z. P. Bažant and P. C. Prat, 'Microplane model for brittle plastic material: I. Theory, II. Verification', *J. Eng. Mech. ASCE*, **114**, 1672–1688, 1689–1702 (1988).
26. J. Ožbolt and Z. P. Bažant, 'Microplane model for cyclic triaxial behavior of concrete', *J. Eng. Mech. ASCE*, **118**, 1365–1386 (1992).
27. J. Ožbolt and M. Petrangeli, 'Improved microplane model for concrete', *Internal Report No. 4/17-93/5*, Institut für Werkstoffe im Bauwesen, Stuttgart University, Germany, 1993.
28. Z. P. Bažant and A. Pfeiffer, 'Determination of fracture energy from size effect and brittleness number.' *ACI Mater. J.*, **84-M41**, 463–480 (1987).
29. D. A. Hordijk 'Local approach to fatigue of concrete', *Dissertation*, Delft, The Netherlands, 1991.
30. Z. P. Bažant and P. Gambarova, 'Crack shear in concrete: crack band microplane model', *J. Struct. Eng. ASCE*, **110**, 2015–2035 (1984).
31. J. G. M. van Mier, 'Scaling in tensile and compressive fracture of concrete, in A. Carpinteri (ed.), *Application of Fracture Mechanics to Reinforced Concrete*, Elsevier Applied Science, Torino, Italy, 95–136 (1992).
32. Z. P. Bažant, 'Distributed cracking and nonlocal continuum', in P. Bergan *et al.* (eds.), *Finite Element Methods for Nonlinear Problems*, Springer, Berlin, 1986, pp. 77–102, also Symp. Preprints, Trondheim 1985, Paper II-2.
33. R. Eligehausen and G. Sawade, 'A fracture mechanics based on description of the pull-out behavior of headed studs embedded in concrete', in L. Elfgren (ed.), *Fracture Mechanics of Concrete Structures—RILEM Report*, Chapman & Hall, London, 1989, pp. 263–280.
34. G. Pijaudier-Cabot and Y. Berthaud, 'Nonlocal damage model for concrete cracking: Identification and inverse analysis', in Folker H. Wittmann (ed.), *Numerical Models in Fracture Mechanics of Concrete*, Swiss Federal Institute of Technology, Switzerland, 1992, pp. 135–156.
35. Z. P. Bažant, T. B. Belytschko and T.-P. Chang, 'Continuum model for strain softening', *J. Eng. Mech. ASCE*, **110**, 1666–1692 (1984).
36. Z. P. Bažant and G. Pijaudier-Cabot, 'Nonlocal continuum damage, localization instability and convergence', *ASME J. Appl. Mech.*, **55**, 287–293 (1988).
37. Z. P. Bažant, Y. Xiang, M. D. Adley, P. C. Prat and S. A. Akers, 'Microplane for concrete: II. data delocalization and verification', *ASCE J. Eng. Mech.*, **122** (1996), in press.